MULTISCIA
JOURNALS PUBLISHERS

FRONTIERS IN PHARMACOLOGICAL RESEARCH

ISSN: (3065- 1379)

https://multisciajournals.com/journals/index.php/fpr

editor.fpr@gmail.com

Frontiers in Pharmacological Research
Volume 1 Issue 4 2025

Isonicotino hydrazide's anti-TB activity: spectroscopic and computational (DFT-SCF) studies

Diego Rivera a,n , Robert Allkin

Department of Pharmacological Research

Article Info

Received: 24-09-2025 Revised:-0312-2025 Accepted:13-12-2025 Published:23-12-2025

1. Introduction

The antibiotic chemical isoniazid, also known as isonicotino hydrazide, is used as a first-line therapy and preventative measure for both active and latent tuberculosis [1]. When it comes to Mycobacteria, especially Mycobacterium tuberculosis, this chemical molecule works well. Additionally, it exhibits activity against certain atypical mycobacteria [2]. There are three types of isonicotino hydrazide: tablets, syrups, and injectables [3–4]. It was thought to be a good place to start when looking for novel active derivatives and analogues, like hydrazones, which have been shown to be effective anti-TB medications [5–6]. Isonicotino hydrazide is a pro drug that requires bacterial catalysis to activate. In particular, hydrazine's reduction of the mycobacterial ferric Kat G catalase-peroxidase and its reaction with oxygen to generate an oxyferrous enzyme complex are linked to activation. Isonicotino hydrazide, once activated, prevents the production of mycoloic acids, which are vital for the bacterial cell wall. Isoniazid is bacteriocidal against Mycobacterium TB organisms that are actively developing both inside and outside of cells at therapeutic concentrations.
An essential part of "triple therapy" to treat tuberculosis is isoniazid. It has decreased the stability of tabletting formulas.
To combat oxidative stress, pulmonary inflammation, and free radical burst from macrophages brought on by tuberculosis and other illnesses, antioxidants are essential. For many years, isoniazid has been the main medication used in clinical settings to treat and prevent tuberculosis. This medication has been regarded as one of the most powerful sensitizing agents, likely able to covalently integrate into a range of protein acceptors in vivo and produce a broad range of hypersensitivity symptoms due to autoimmunization.

Introduction

Isoniazid's basic organic structure includes two crucial elements—a pyridine ring and a hydrazide group—that are necessary for its potent action against Mycobacterium tuberculosis [7-8]. Mycolic acids are a crucial part of the bacterial cell wall, and isoniazid prevents their formation. Isoniazid is bactericidal against intracellular and extracellular MTB pathogens that are actively proliferating at therapeutic concentrations. Under multi-drug therapy, isoniazid is used in combination with other potent anti-tuberculosis medications [9].
After reviewing the literature, it was discovered that no research had been done to employ a spectroscopic instrument backed by computer calculations to examine the underlying mechanism of the compound's anti-TB activity. FT-IR, FT-Raman, NMR, and UV-visible spectral analyses have been performed in the current study to provide the pharmacological activity.

2. Profile of experiments

Physical state: • The pure, spectroscopic-grade chemical was taken in solid form.

Recording profile: • A Bruker IFS 66V spectrometer was used to record the compound's FT-IR and FT-Raman spectra. The device was fitted with a FRA 106 Raman module that had an aNd:YAG laser source that operated at 1.064 µm line widths with 200 mW power [10].
• FT-NMR spectrometers operating at 300 MHz and 75 MHz were used to record the high resolution 1HNMR and 13CNMR spectra [11].
• Using the UV-1700 series equipment, the UV-Vis spectra was acquired between 200 and 800 nm with a 0.2 nm scanning interval [12].

3. The profile of computation

The current molecule was created with optimal geometry using Gauss view, and the program was executed using this geometry. All of the calculations were completed in order to determine the parameters that were utilized for various aspects of analysis. The vibrational spectral features, Mulliken charge levels, and geometrical parameter changes were tabulated for the adjustment of physical and chemical parameters in the composite molecule created by base and substitutional combinations. The Gaussian 09 D. 01. version software application on a core i7 computer was used to carry out all of the quantum chemistry calculations [13].
Computational computations were conducted utilizing the B3LYP and B3PW91 methods using the 6-31++G(d, p) and 6-311++G(d, p) basis sets to determine unknown geometrical parameters, vibrational frequencies, molecular structure modeling, and spectra. The time-dependent SCF approach with best fit basis set was used to compute the energy absorbance by the current chemical in relation to electronic spectra, the NBO, and the HOMO-LUMO energies. Similarly, the GIAO approach was used to calculate the 1H and 13C NMR chemical shifts with respect to TMS utilizing the I-PCM model in conjunction with B3LYP/6-311++G(d,p). The Mullikan charge assignment on several components of the compound was computed and deliberately clarified in order to identify a crucial component for the compound's pharmacological activity. Using the 6-311++G(d,p) basis set and the B3LYP method, the dipole moment, linear Polarizability, and first order hyper-Polarizability in several coordinate systems of the compound were calculated. The optical chirality was examined, the method for hiding the toxicity was deciphered, and the ECD and VCD spectra were simulated using available frequencies.

4. Findings and conversation

4.1. Analysis of structural deformation

Figure 1 showed the density of energy levels for the bond type of the current molecule. The current chemical was created by substituting carbonyl and amine groups for the pyridine ring. The essential frame of the molecule is typically modified as a result of the substitutions [14]. As a result, it was discovered that the pyridine ring in this instance was shattered similarly to the replacements.
The ring without substations has the following bond length values: C1-C2: 1.393, C1-N6: 1.336, C2-C3: 1.391, C3-C4: 1.391, C4-C5: 1.393, and C5-N6: 1.336. In contrast, the identical bond length of the ring's C-C and C-N with replacements was, successively, C1-C2: 1.389, C1-N6: 1.334, C2-C3: 1.392, C3-C4: 1.394, C4-C5: 1.392, and C5-N6: 1.331. Based on this sequence, it was discovered that the bond lengths were reduced by up to 0.004 Å in the cases of C1-C2 and C4-C5. However, the changes resulted in a 0.003Å increase in the bond lengths C2-C3 and C3-C4. The bond length was reduced to 0.005Å in the cases of C1-N6 and C5-N6. The ligand group's insertion was the cause of all these asymmetric bond length changes. Both physical and chemical properties changed as a result of such changes in physical parameters. As a result, the pyridine compound's primary characteristic was that it was an antipyretic; nevertheless, following substitution, the current compound functioned as an antituberculosis drug.
Because of the hetero nuclear atom, the bond angles C2-C1-N6 and C4-C5-N6 were nearly equal to 123.7°, which was a very high stretching semicircle angle in the ring. The insertion of chain significantly reduced the bond angle C2-C3-C4 to 117.8°. The associated mass and energy of the chain were fully transferred to the ring after this condition was resolved. Thus, in relation to the ligand group, the pyridine ring's chemical properties were totally changed. Figure 1 showed the density of energy states diagram for the current chemical. The energy spectrum density was noticeably intensely accumulated at the ligand group's location over the ring, according to the figure. The discrete energy levels were orientated at the top end of the

energy spectrum, while the energy of the vacant level was located at the tail end. The energy transfer from the ligand group to the pyridine ring was visible in this image.

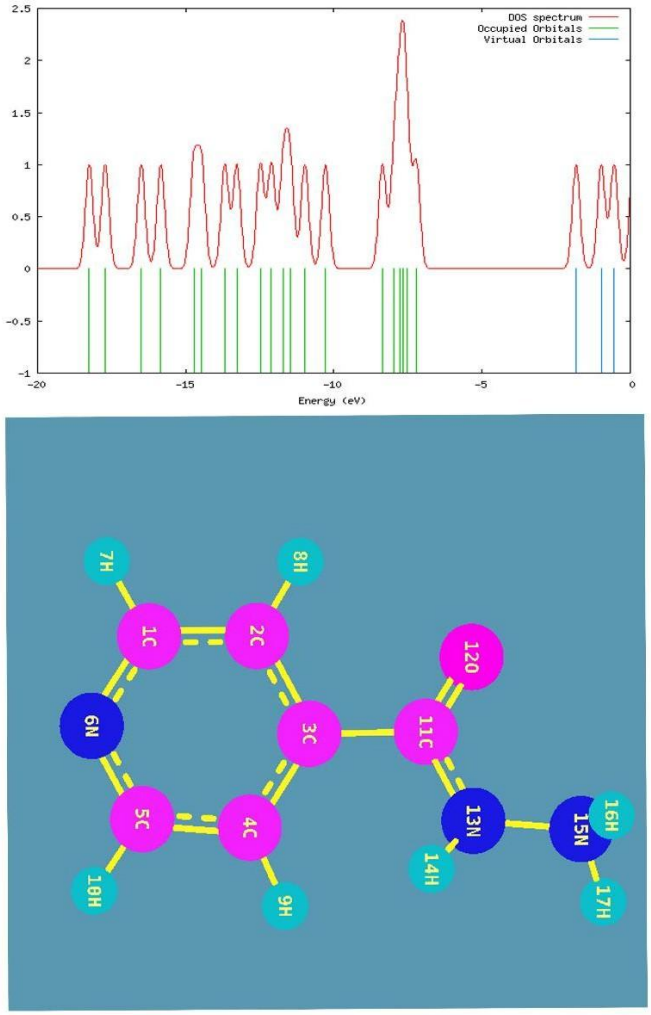

Geometrica+A +A1:F26	Methods				
Parameters	HF	B3LYP		B3PW91	
	6-311++G (d, p)	6-31++G (d, p)	6-311++G (d, p)	6-311++G (d, p)	6-31++G (d, p)
Bond length(Å)					
C1-C2	1.383	1.391	1.394	1.389	1.392
C1-N6	1.32	1.338	1.341	1.334	1.338
C1-H7	1.076	1.086	1.087	1.087	1.088
C2-C3	1.385	1.395	1.398	1.392	1.396
C2-H8	1.072	1.082	1.084	1.083	1.085
C3-C4	1.386	1.397	1.4	1.394	1.398
C3-C11	1.51	1.511	1.511	1.506	1.507
C4-C5	1.386	1.394	1.397	1.392	1.395
C4-H9	1.074	1.083	1.085	1.085	1.086
C5-N6	1.317	1.334	1.338	1.331	1.335
C5-H10	1.076	1.086	1.087	1.087	1.088
C11-O12	1.187	1.212	1.22	1.21	1.217
C11-N13	1.363	1.377	1.378	1.372	1.374
N13-H14	0.994	1.011	1.013	1.011	1.012
N13-N15	1.383	1.397	1.397	1.387	1.388
N15-H16	0.998	1.014	1.015	1.013	1.014
N15-H17	0.997	1.012	1.014	1.012	1.012
Bond angle(º)					
C2-C1-N6	123.596	123.698	123.748	123.781	123.82
C2-C1-H7	120.128	120.24	120.245	120.207	120.21
N6-C1-H7	116.274	116.06	116.006	116.011	115.96
C1-C2-C3	118.488	118.842	118.827	118.765	118.75
C1-C2-H8	121.076	121.324	121.369	121.471	121.49
C3-C2-H8	120.433	119.831	119.802	119.762	119.74
C2-C3-C4	118.142	117.831	117.844	117.883	117.89
C2-C3-C11	118.304	118.125	118.129	118.064	118.06
C4-C3-C11	123.535	124.01	123.998	124.017	124.00
C3-C4-C5	118.443	118.769	118.754	118.685	118.66
C3-C4-H9	121.901	121.687	121.691	121.69	121.69
C5-C4-H9	119.625	119.503	119.514	119.58	119.58
C4-C5-N6	123.573	123.677	123.726	123.764	123.80
C4-C5-H10	120.019	120.125	120.128	120.093	120.10
N6-C5-H10	116.406	116.196	116.144	116.141	116.08
C1-N6-C5	117.743	117.165	117.088	117.102	117.03
C3-C11-O12	121.134	121.613	121.539	121.656	121.57
C3-C11-N13	114.025	113.835	114.068	113.627	113.87
O12-C11N13	124.84	124.55	124.392	124.716	124.55
C11-N13H14	117.941	118.27	118.27	118.1	118.16
C11-N13N15	120.138	120.474	120.277	120.572	120.36
H14-N13-N15	118.741	119.49	119.403	119.807	119.70
N13-N15-H16	111.729	111.532	111.669	111.604	111.81
N13-N15-H17	110.351	110.378	110.381	110.563	110.65
H16-N15-H17	110.95	110.698	110.939	110.676	111.02
Dihedral angle(º)					
N6-C1-C2C3	-0.895	-0.936	-0.771	-0.983	-0.876
N6-C1-C2H8	178.745	178.654	178.784	178.621	178.71
H7-C1-C2C3	179.354	179.291	179.393	179.245	179.34
H7-C1-C2H8	-1.004	-1.118	-1.051	-1.15	-1.106
C2-C1-N6-C5	-0.105	-0.163	-0.24	-0.187	-0.256
H7-C1-N6-C5	179.653	179.617	179.601	179.592	179.57
C1-C2-C3-C4	1.163	1.324	1.211	1.411	1.304
C1-C2-C3-C11	179.683	179.317	179.388	179.351	179.39
H8-C2-C3-C4	-178.479	-	-178.35	-178.2	-
H8-C2-C3-C11	0.039	-0.278	-0.174	-0.26	-0.163
C2-C3-C4-C5	-0.513	-0.696	-0.707	-0.754	-0.748
C2-C3-C4-H9	177.518	177.015	177	176.859	176.83
C11-C3-C4-C5	-178.949	-	-178.767	-178.561	-
C11-C3-C4-H9	-0.917	-0.848	-1.06	-0.947	-1.129
C2-C3-C11-O12	-31.198	-28.884	-28.439	-29.44	-
C2-C3-C11-N13	148.778	150.969	151.554	150.304	150.62
C4-C3-C11-O12	147.235	148.974	149.615	148.363	148.72
C4-C3-C11-N13	-32.788	-31.171	-30.39	-31.892	-31.41
C3-C4-C5-N6	-0.515	-0.423	-0.321	-0.44	-0.367
C3-C4-C5-H10	179.288	179.234	179.328	179.225	179.28
H9-C4-C5-N6	-178.593	-178.186	-178.079	-178.105	-178.01
H9-C4-C5-H10	1.211	1.48	1.57	1.56	1.647
C4-C5-N6-C1	0.827	0.856	0.797	0.914	0.871
H10-C5-N6-C1	-178.983	-178.822	-178.865	-178.763	-178.8
C3-C11-N13-H14	-18.176	-14.393	-15.594	-13.414	-14.557
C3-C11-N13-N15	-177.786	-179.188	-179.223	-179.323	-179.39
O12-C11-N13-H14	161.798	165.455	164.399	166.321	165.30
O12-C11-N13-N15	2.189	0.66	0.77	0.411	0.472
C11-N13-N15-H16	103.485	105.897	104.7	106.827	105.59
C11-N13-N15-H17	-132.571	-130.604	-131.391	-129.518	-130.09
H14-N13-N15-H16	-55.962	-58.713	-58.744	-58.843	-59.008
H14-N13-N15-H17	67.98	64.784	65.164	64.81	65.307

Table 1: Optimized geometrical parameters for Isonicotinohydrazide computed at HF/DFT (B3LYP&B3PW91) with 6-31++G(d, p) & 6-311++G(d, p) basis sets.

1.1. Mulliken charge dislocation analysis

The molecular orbital formation is decided by symmetrical and asymmetrical charge distribution among atoms [15]. The symmetry or asymmetry of the charge distribution plays a fundamental role in determining the chemical properties of the molecule and consequently this property of the charge distribution is used as a basis for the classification of chemical bonds [16-17]. All the chemical bonds in the compound would be formed as covalent bond between composite atoms and are to be polar and non polar. Normally, in the compound, the polar and non polar bonds are existed with respect to the substitutional groups. If the ration of polar bonds is greater, the asymmetry charges distribution taking place in the compound. Here, the dipole moment of the compound was found to be high since the ratio of hetero nuclear bonds was greater than homo nuclear bonds. The Mulliken charge levels were depicted in the Table 2 and the corresponding pictorial diagram was shown in Figures 2 and 3.

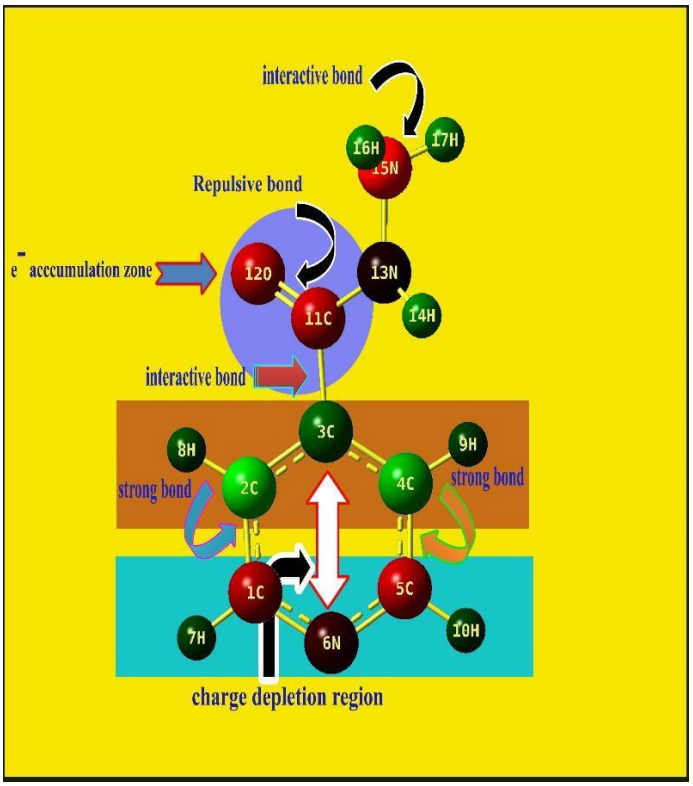
interactive bond
16H
17H
15N
Repulsive bond
e⁻ acccumulation zone
12O
13N
11C
14H
interactive bond
3C
8H
9H
strong bond
2C
4C
strong bond
1C
5C
7H
6N
10H
charge depletion region

S. No.	Atom Position	Mullikan charge	
		B3LYP	B3PW91
1	**C1**	-0.563	-0.758
2	**C2**	0.324	0.440
3	**C3**	0.665	0.691
4	**C4**	0.112	0.230
5	**C5**	-0.571	-0.771
6	**C11**	-0.599	-0.716
7	**H7**	0.179	0.215
8	**H8**	0.223	0.260
9	**H9**	0.193	0.234
10	**H10**	0.172	0.207
11	**012**	-0.288	-0.274
12	**N6**	-0.046	0.006
13	**N13**	-0.141	-0.105
14	**H14**	0.246	0.262
15	**N15**	-0.389	-0.426
16	**H16**	0.246	0.258
17	**H17**	0.238	0.247

Table 2: Mulliken Charge levels of Isonicotinohydrazide at different methods

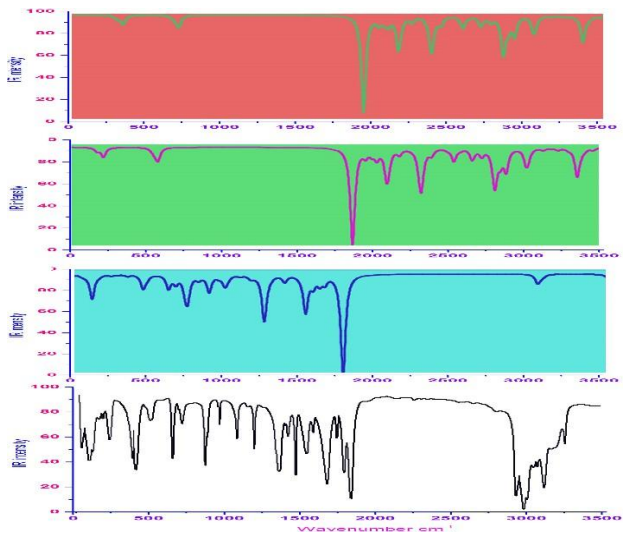

In this compound, though the hetero nuclear atom (N) present in the ring, the strong bond was created between CC of the ring and also the N was to be found as neutral. Due to the asymmetrical charge dislocation motion towards substitutional group, the top moiety of the ring becomes protonic region whereas the bottom moiety turns out to be electron rich region (depletion region). From this view, it was inferred that, the considerable amount of chemical energy was transferred from ring to ligand group. Normally, the rich polar character present in carbonyl group, but in this case, the electronic charges were accumulated vigorously and the bond come in to repulsive. On the other side of the substitutional group, in order to make strong attractive bond, the intermediate nitrogen atom converted as neutral.

1.2. Vibrational analysis

1.2.1. Vibrational assignments

The fundamental frequency pattern of the compound was represented by IR and Raman spectra and the observed spectral peaks in terms of wavenumbers were presented in the Table 3 and the observed with simulated FT-IR and FT-Raman spectra were presented in the Figure 4&5. According to the vibrational degrees of freedom, since the present compound contained 17 atoms, there were 45 fundamental modes of vibrations were observed. Out of 45 vibrational modes, 17 stretching, 14 in plane and 14 out of plane bending modes were distinguished. Since the title molecule was non Centro-symmetry, the vibrations are active in IR and those inactive in Raman and vice versa. The total elementary vibrations were ordered as **Γ= 31A′+ 14A″**

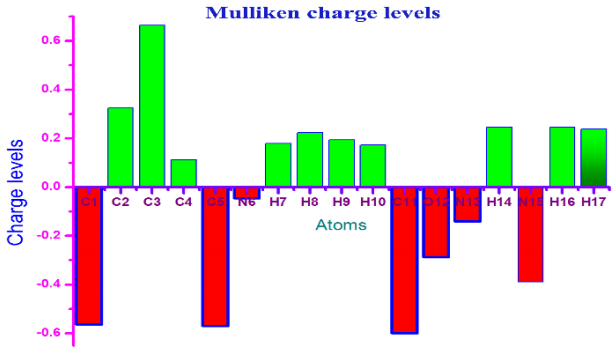

C-H vibrations

Normally, the ring C-H vibrations in benzene and pyridine ring ensured that, whether the hexagonal frame has substituted by ligand or not. If the observed fundamentals are observed within the expected region, the ring will not be affected much by the substitutions. Otherwise, the ring vibrations are rather suppressed and ratio of the same showed the impact of the substitutions on the ring. Here, the substitutional group was present at one C of the ring and 16 C-H vibrations are possible. Accordingly, the C-H stretching vibrations were found at 3070, 3040, 3010 and 2990 cm^{-1} in IR and Raman spectra. The in plane and out of plane bending vibrations were observed at 1060, 1050, 1010 and 1005 cm^{-1} and 720, 665, 660 and 650 cm^{-1} respectively. The hetero aromatic C H stretching vibrations are normally found between 3100 and 3010 cm^{-1}, the C–H in plane bending frequencies appear in the range of 1000 - 1310 cm^{-1} and C–H out of plane bending vibration in the range 750 - 1000 cm^{-1} [18-20]. The entire vibrational bands are expected to observe with medium to strong intensity. But all the bands were found with very week to very strong intensity. One peak of stretching and entire signals of out of plane bending were observed out of the expected region whereas all the in plane bending modes were found at the top end of the allotted region. The observed signals were affected in low energy region which was mainly by the energy transformation from ring to ligand group in order to generate anti-tuberculosis activity.

1.2.2. Ring CC and C-N vibrations

The main hexagonal frame of pyridine ring is constituted by C-C bonds and these are directly affected by the loaded ligand groups. In addition to that, the ring associated with N atom, so the ring vibrations include the C=N and C-N vibrations also. Interactions between ring C=C and C=N stretching vibrations result in two strong-to-medium intensity absorptions about 100 cm^{-1} apart [21]. Usually, the C=C and C=N stretching modes are observed in the region 1615-1575 cm^{-1} and 1520 -1465 cm^{-1} respectively [22- 25]. Accordingly, in the present case, the C=C and C=N stretching signals appeared at 1660 & 1630 and 1580cm^{-1} respectively. Both the stretching bands are moved well above the expected level of the spectrum. In this view, it was cleared that, the ring energy was found to be increased and which was favor for the energy transaction between ring and ligand group. Usually, these vibrations are followed by C-C and C-N stretching bands which are observed around 1460 cm^{-1}[26]. In this case, these vibrational bands were observed at 1530 cm^{-1} and 1490 & 1430 cm^{-1} respectively. The CCC and CNC in plane and out of plane bending (ring breathing) modes were identified at 300, 225& 175 and 135, 120 & 50 cm^{-1}

respectively. These observed fundamental modes moved down to well below the expected region. The ring deformation vibrations have been restricted since it was substituted by the carbonyl and amino groups. Finally, it was concluded that, the ring energy was consumed lot for the formation of drug property.

S. No	Symmetry Species	Observed Frequency(cm-1)		Methods					Vibrational
	C_S			HF	B3LYP		B3PW91		Assignments
		FT-IR	FT-Raman	6-311++G (d,p)	6-31++G (d,p)	6-311++G (d,p)	6-31++G (d,p)	6-311++G (d,p)	
1	A′	3480m	-	3474	3474	3466	3473	3489	**(N-H) υ**
2	A′	3460m	-	3472	3476	3466	3463	3447	**(N-H) υ**
3	A′	3360m	-	3354	3342	3375	3367	3356	**(N-H) υ**
4	A′	-	3070w	3051	3075	3061	3057	3063	**(C-H) υ**
5	A′	-	3040vw	3033	3053	3040	3034	3042	**(C-H) υ**
6	A′	3010vs	-	3011	2999	3016	3014	3018	**(C-H) υ**
7	A′	2990s	-	2980	2992	2990	3007	2990	**(C-H) υ**
8	A′	1750m	-	1758	1750	1746	1756	1750	**(C=O) υ**
9	A′	-	1660vw	1657	1659	1660	1665	1661	**(C=C) υ**
10	A′	-	1630vw	1624	1630	1625	1631	1634	**(C=C) υ**
11	A′	1580s	-	1583	1579	1572	1580	1572	**(C=N) υ**
12	A′	1530w	-	1535	1525	1524	1533	1528	**(C-C) υ**
13	A′	1490w	-	1486	1496	1493	1486	1496	**(C-N) υ**
14	A′	1400w	-	1402	1407	1399	1397	1402	**(C-N) υ**
15	A′	1320vs	-	1320	1320	1316	1316	1325	**(C-C) υ**
16	A′	-	1290vw	1286	1290	1295	1291	1285	**(C-C) υ**
17	A′	-	1270vw	1272	1267	1265	1271	1275	**(N-H) δ**
18	A′	-	1210vw	1209	1213	1215	1210	1210	**(N-H) δ**
19	A′	1190vw	-	1183	1190	1189	1193	1188	**(N-H) δ**
20	A′	-	1130m	1134	1130	1130	1130	1130	**(N-N) υ**
21	A′	-	1060vw	1061	1061	1060	1062	1058	**(C-H) δ**
22	A″	1050w	-	1053	1052	1053	1046	1054	**(C-H) δ**
23	A″	-	1010vs	1015	1005	1011	1009	1013	**(C-H) δ**
24	A′	-	1005m	1004	1005	1007	1007	1007	**(C-H) δ**
25	A′	-	1000m	997	999	1001	998	997	**(C=O) δ**
26	A′	975vs	-	974	977	977	976	973	**(C-N) δ**
27	A′	-	900w	902	899	903	901	897	**(C-C) δ**
28	A′	885w	-	888	882	881	883	881	**(N-H) γ**
29	A″	855s	-	856	872	877	872	877	**(N-H) γ**
30	A″	-	765vw	763	767	762	762	763	**(N-H) γ**
31	A″	750w	-	753	746	753	750	752	**(N-N) δ**
32	A″	720vw	-	719	735	721	717	721	**(C-H) γ**
33	A″	-	665w	665	664	664	668	664	**(C-H) γ**
34	A″	-	660w	660	661	657	660	661	**(C-H) γ**
35	A″	550vw	-	550	548	550	553	555	**(C-H) γ**
36	A″	-	510vw	509	512	510	509	512	**(C=O) γ**
37	A″	-	405w	406	406	406	404	404	**(C-N) γ**
38	A″	-	390vw	391	396	395	391	391	**(C-C) γ**
39	A″	-	350vw	350	350	350	351	351	**(CNC) δ**
40	A′	-	300vw	300	299	301	300	299	**(CCC) δ**
41	A′	-	225vw	225	224	226	225	225	**(CCC) δ**
42	A′	-	175m	175	173	176	177	175	**(N-N) γ**
43	A″	-	135s	134	135	135	135	135	**(CCC) γ**
44	A″	-	120m	120	116	115	115	116	**(CNC) γ**
45	A″	50m	-	50	50	50	50	50	**(CCC) γ**

Table 3: Observed and calculated vibrational frequencies at HF and DFT (B3LYP & B3PW91) with 6-31++G(d,p) & 6-311++G (d,p) level for Isonicotino hydrazide VS –Very strong; S – Strong; m- Medium; w – weak; as- Asymmetric; s – symmetric; υ – stretching; α –deformation, δ - In plane bending; γ-out plane bending; τ – Twisting:

1.2.3. NH_2 vibrations

Specifically, the amino group is always dominating all other groups and it very much pronounced in the drug property of the compound [27]. In this case also, the amino group was played important role to induce such anti-tuberculosis activity. Usually, the N-H stretching modes are appeared in the region 3300-3500 cm^{-1}[28-29]. Therefore, the same signals for N-H stretching found with medium intensity at 3480, 3460 and 3360 cm^{-1} in IR only. As in the previous case [30], such vibrations were observed at the top end of the allocated area. Form this observation, it was cleared that, these components were found to be active and it took part in transaction of energy for creating novel property.

The N-H in-plane bending vibrations (scissoring) are usually observed in the region 1610-1630cm^{-1} and the out of plane bending (wagging) vibrations are normally identified in the region 1150-900cm^{-1} [31-32]. Here, these vibrations (in plane and out of plane) have been observed at 1270, 1210 & 1190 cm^{-1} and 885, 855 & 765 cm^{-1} respectively. Dissimilar to the stretching, these bending modes were found to be affected and depressed much which was due to the presence of carbonyl group. The activeness of bending modes rather decreased by C=O group by inductive effect.

2.4. C=O, N-N and C-C vibrations

The ketones related Carbonyl group vibrations are the important characteristic bands in vibrational spectra since it acts as major part of creating complete property and therefore, these bands have been the subject of wide analysis [33-34]. Normally, the intensity of these bands would be greater since its conjugation and dipole moment. Therefore, it leads to the intensification of the scattering lines as well as very strong intensity of infrared band. The carbonyl stretching vibrations in ketones are expected in the region 1680–1715 cm^{-1}[35]. In this case, a band was found with medium intensity at 1750 cm^{-1} in IR only. The band was appeared well above the allowed region but its intensity was suppressed which was due to the nearby amino group. It's in plane and out of plane bending vibrational modes were observed at 1000 and 405 cm^{-1} respectively. These vibrational modes were agreed well with the previous work [36].

The amine groups were attached with one another by N-N bond and forming azine group and it was very significant since it is Y-junction which exchanges the energy between ring and amine group of molecule. Generally, the azine bond N-N stretching vibration was found around 925-1150 cm^{-1} [37]. The N-N stretching vibration was observed with medium intensity at 1130 cm^{-1}. The consequent in plane and out of plane bending modes were observed at 750 and 175 cm^{-1} respectively. The acquired vibrational bands were precisely harmonized with the literature and ensure the role of azine group in the drug properties of the compound.

The C-C stretching of C-C bond of out of the ring are observed in the region 1470-1520 cm^{-1}[33]. Here, the stretching modes have been found at 1320 and 1290 cm^{-1}. The corresponding in and out of plane bending vibrations was observed at 885 and 390cm^{-1} respectively. These bands were at exact allowed region since it was favored by the carbonyl and amino groups.

2.3. NMR confinement

The ^{1}H and ^{13}C NMR spectral data was presented in Tables 4 and the corresponding spectra were shown in Figure 6. Generally, the chemical shift of carbons and hydrogens are situated in different environment with respect to the coupling constant and makes the molecule complicated. The isotropic chemical shift of C and H are usually explicated the unknown chemical properties of complicated compound. In general, the chemical shifts of carbon is depends upon the bonded atoms and their chemical environment in the compound. The isotropic chemical shifts in aromatic compounds are universally observed in the region of 100-190 ppm [38]. The chemical shift of C of base compound with respect to ligand attachment is providing direct the dependable interpretation of chemical properties. Usually, the chemical shift of aliphatic chain is constantly behind the aromatic compound [39]. Symmetry also makes atoms equivalent in molecules and if group of atoms are in some identical locations relative to a plane of symmetry in a molecule, they will be equivalent [40-41]. Here, the carbons of the ring were located in the region 140- 160 ppm as in normal case.

Generally, the NMR signals are falling into domain with respect the diamagnetic equivalence of carbon and hydrogen atoms. The observed chemical shift of carbons of the pyridine ring; C1, C2, C3, C4 and C5 were restricted in the region 140-164 ppm. The observed chemical shift of C1 and C5 were found to be same (164ppm) which was more than rest of others due to coupling of N whereas the calculated shift was 156 and 158 ppm respectively. This condition also due to the asymmetrical electron orientation on such carbons which was evident in Mulliken charge analysis. Similarly, C2 and C4 were same and 140 ppm, but the observed and calculated chemical shift of C3 was 150 and 144 ppm respectively. The observed and calculated chemical shift of C11 was found to be 170 195 ppm respectively which is greater than others since its electron cloud was fragmented asymmetrically by ring, carbonyl and amino groups. The C3 and C11 have been opened up due to the random breaking of proton shield by π-bonded oxygen and amine groups in which the consistent amount of energy was exchanged among different entity of molecule in order to enforce the drug property in the compound.

The hydrogen atoms were attached with C and N atoms in the molecule which make different environment upon which the chemical shift of the atoms was classified. Here, the chemical shift of H in ring was observed in the region 7- 10 ppm whereas in amino group, the shift was observed 4.5 and 7.6 ppm. The chemical shift was observed consistently with respect to the attached atoms.

Atom position	**TMS-B3LYP/6-311+G(2d,p) GIAO Shift in (ppm)**			Experimental shift **(ppm)**
	Gas	**Solvent phase**		
		DMSO	**CCl4**	
1C	158.169	157.891	158.165	164.0
2C	127.195	127.078	127.208	140.0
3C	144.129	144.814	144.388	150.0
4C	123.629	126.602	124.698	140.0
5C	156.024	157.095	156.448	164.0
11C	195.801	200.559	197.758	170.0
6N	389.791	374.241	383.229	-
13N	148.607	153.23	150.436	-
15N	72.7634	70.778	71.9611	-
7H	9.2127	9.2304	9.2313	8.7
8H	7.8878	7.9	7.9044	7.8
9H	6.9857	7.4784	7.1771	7.8
10H	9.0101	9.1184	9.0566	10.0
14H	6.3622	6.9062	6.5681	7.6
16H	2.1522	2.4561	2.2692	4.5
17H	2.6703	3.1309	2.8651	4.5
12O	545.715	489.285	522.323	-

Table 4: Experimental and calculated ^{1}H and ^{13}C NMR chemical shifts (ppm) of isonicotinohydrazide

1.4. Frontier molecular outline

The interaction between two atomic or molecular orbitals will form two new orbitals. One new orbital is antibonding orbital which has the higher energy than the original molecule orbital. The other new orbital is the bonding orbital which is lower in energy than the initial one. The stabilization of the bonding molecular orbital and destabilization of the antibonding can increase when the overlap of two orbitals increases [42]. In the molecular interaction, there are the two important orbitals interact each other. One is the highest energy occupied molecular orbital is called HOMO. The other one is the lowest energy unoccupied molecular orbital is called LUMO. When a pair of electrons filled in one of the molecule orbital and no electron occupy in the other orbital, this interaction is very stable and called filled- empty interaction.

The orbital interaction profile of title compound was presented in the Figure 7 in which different bonding interactions were seen clearly. The elevated orbital energy level was depicted in the Table 5. In the case of LUMO, there were two sets of first order π-bonding interaction found over the ring cc of opposite moiety and one σ-bonding existed on N of the ring. Apart from that, one π-bonding interaction taking place between ring C and ligand C which was also connect =O. one N-H iso surface was observed and little flavor was identified on H. usually, the π-conjugation interaction orbitals induce active biological as well as crystal property in the aromatic compound[43]. Here, the electron cloud receiving location (LUMO) was observed to be π-orbital overlapping region where the orbital was degenerative and able to consume electronic energy from HOMO.

In HOMO, the cascade of orbital overlapping of degenerate energy levels at top and bottom moiety of the ring which connect CNC and CCC with two H. peculiarly, the δ-bond orbitals found at C3 of ring C11, O12 and N13 of ligand chain. The δ-bond interaction is very rare and if present in compound, there will be stimulation of drug activity. Here, from the orbital interaction, proved the anti tuberculosis action of the present compound. In second order orbital interaction (HOMO+1 and LUMO-1), the positive and negative intersection was found and all the degenerate energy levels were interacted to make centralized donor region for supplying electronic energy.

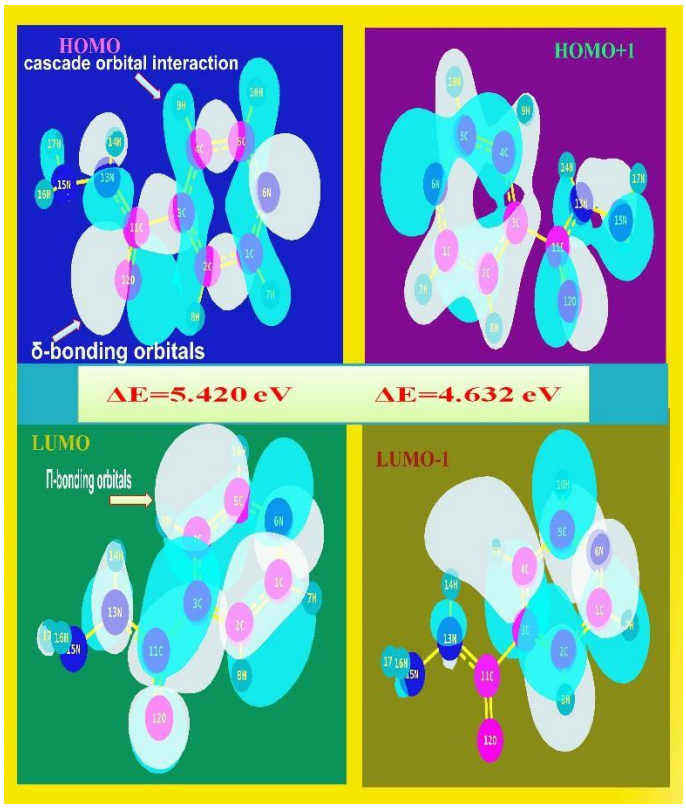

Energy levels	IR Region Energy in eV	UV-Visible region Energy in eV
H+10	12.17545	12.44077
H+9	11.72184	11.72402
H+8	11.54225	11.66633
H+7	10.99285	10.8938
H+6	10.3708	10.72155
H+5	8.35498	8.86002
H+4	8.02245	8.39743
H+3	7.79279	7.88613
H+2	7.70762	7.8064
H+1	7.57238	7.37319
H	7.28312	7.01999
L	1.86261	2.38725
L-1	1.03593	1.27403
L-2	0.82178	0.79919
L-3	0.14966	0.17252
L-4	0.18422	0.06721
L-5	0.31946	0.19837
L-6	0.51783	0.52164
L-7	0.74722	0.56273
L-8	0.92545	0.93389
L-9	1.21444	1.14695
L-10	1.30614	1.35703

Table5 :Frontier Molecular orbitals and Energy Level

1.5. UV-Visible absorption analysis

UV-Visible spectral analysis provides the information regarding the ligand group which causing the outstanding chemical property of the compound. Normally, the substitutional impact shifts the electronic excitation pattern (finger print region) of the base compound. The electronic excitation parameters are presented in the Table 6 and the absorption band was displayed in the Figure 8. Here the compound architected by pyridine ring attached with amino group and carbonyl group. Generally, the pyridine ring absorbance peak identified at 190 nm with 76 Kcal/mol in the UV-Visible spectrum [44]. But, by the addition of the substitutional group, the UV band was found at 331 nm with the transition energy of 86.34 Kcal/mol by crossing the energy gap of 3.74 eV. The oscillator strength of the oscillation (transition between ground and excited state) was found to be 0.0134 with higher molar absorptivity. The shift was represented as bathochromic for the higher wavelength region. Usually, the presence of chromophores such as C=O and NH2, enable intensive absorption bands at 290 and 280 nm respectively [45]. In this case, the triplet absorption bands were appeared at 331, 319 and 293 nm with effective intensity. These absorption peaks ensure the presence of such chromophores which was the reason for the inducement of the anti tuberculosis activity.

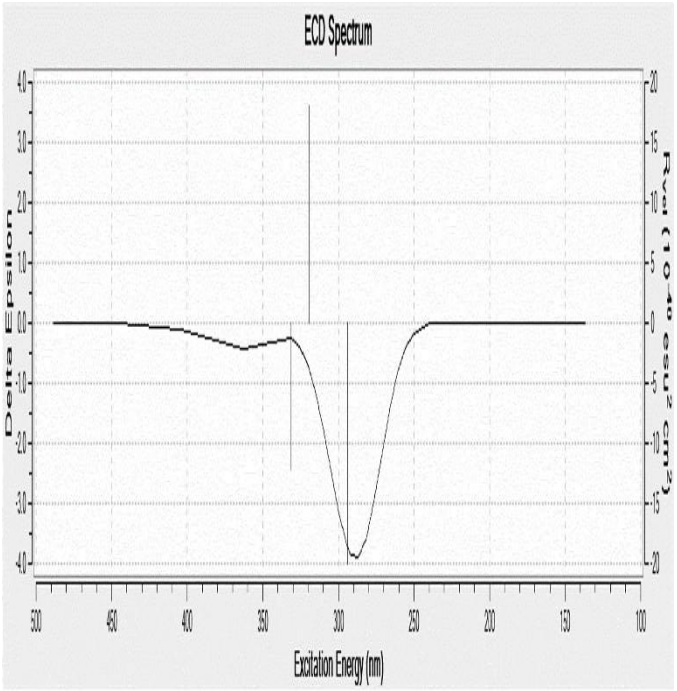

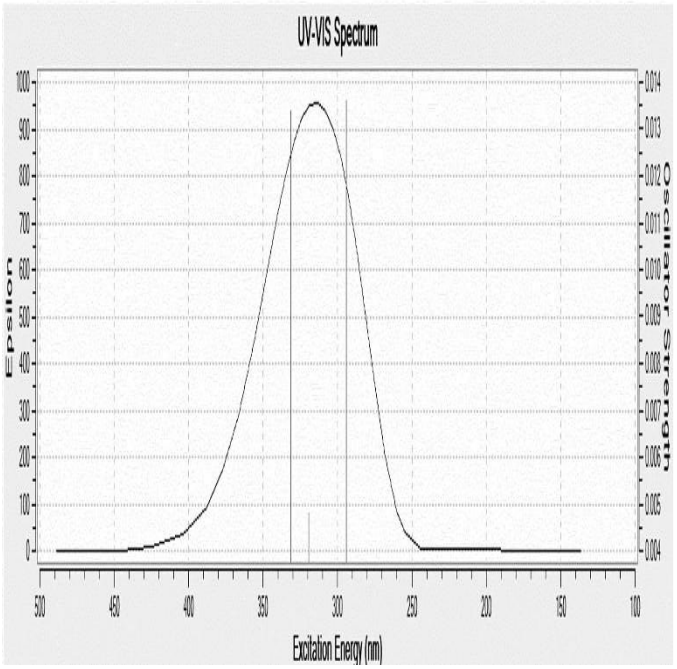

The entire transitions in the electronic HOMO and LUMO energy levels were found to be confined within the quartz UV region of the spectrum which implies that, the title compound would not be active in visible region. Because of this condition of the compound, the drug may be inert for light radiation. The UV-Visible frontier molecular excitations were belonging to n→π* class of transitions showed the strong interaction between donor (carbonyl and amine groups) and acceptor (pyridine ring). The absorption band for title compound was transparently taking place in the UV spectrum in R-band (German, radikalartig) and constantly being with therapeutic activity. In this case, the identification of absorption band in quartz-UV region predicted that, the functional group of amine and azine entities at ring was played significant role for the inducement of pharmaceutical action.

The electronic charge distribution is responsible for electronic polarization of orbitals which was induced by local electric field called ECD. The interaction of chromophores on the base compound making two fold of energy increments for transition to excited states adjust the chemical activity of the compound which can be identified in the ECD spectra. As in the Figure 8, the ECD absorption band was identified at 290 nm which was the characteristic band of C=O and NH2 groups. This band represents uniqueness effect of chemical reactivity.

λ (nm)	E (eV)	(*f*)	Energyin Kcal/mol	Major contribution	Assignment	Region	Bands
Gas							
331.13	3.7443	0.0134	86.34	H_ L (95%)	n→π*	Quartz UV	R band (German, radikalartig)
319.33	3.8826	0.0048	89.53	H_ L (85%)	n→π*	Quartz UV	
293.95	4.2179	0.0136	97.26	H_ L (95%)	n→π*	Quartz UV	
DMSO							
324.8	3.8172	0.0359	88.02	H_ L (85%)	n→π*	Quartz UV	R band (German, radikalartig)
313.14	3.9594	0.0039	91.3	H_ L (92%)	n→π*	Quartz UV	
285.44	4.3436	0.0096	100.16	H_ L (95%)	n→π*	Quartz UV	
CCl_4							
328.88	3.7699	0.0253	86.93	H_ L (85%)	n→π*	Quartz UV	R band (German, radikalartig)
317.46	3.9055	0.0054	90.06	H_ L (92%)	n→π*	Quartz UV	
291.76	4.2495	0.0134	97.99	H_ L (95%)	n→π*	Quartz UV	

Table 6: Theoretical electronic absorption spectra of Isonicotino hydrazide(absorption symbols λ (nm), excitation energies E (eV) and oscillator strengths (f)) using TD-DFT/B3LYP/6-311++G(d,p) method

1.6. Molecular electrostatic potential (MEP) maps

The molecular electrostatic potential is asymmetric charge distribution in different entities of a molecule. The molecular interaction energy was calculated by using the equation

$$V(r_1) = \sum_{j=1}^{M} \lfloor_{1} \quad _{j} \rfloor$$

$$\frac{Qi}{\lceil r - r}$$

If the charge distribution continuous over the compound, the MEP is then given by equation at any instant

$$V(r) = \int_{1} \frac{\rho(r)}{} dr$$

$$1 \qquad [r - r]$$

The MEP is highly informative concerning the protonic and electronic charge distribution of a given molecule. It is mainly used for asymmetric charge orientation among different atoms causing strong electrostatic potential between two extreme charge levels which is favor for the inducement of the particular biological and pharmaceutical properties. The framed Molecular electrostatic potential view was presented in Figure 9 in which the entire molecular interactive zones can be viewed. The static potential energy interaction generated between proton and electron fields is ranged from high frequency (blue) region to higher wavelength (red) region which designated that, the charge dislocation between electrophilic and nucleophilic boundaries. In a molecule, charges are polarized rigorously in negative and positive terminals, and there are significant differences in electron and proton density due to the injection of substitution in base compound. The rich electro negativity region was indicated by wealthy red and positive (proton region) almost was indicated by blue.

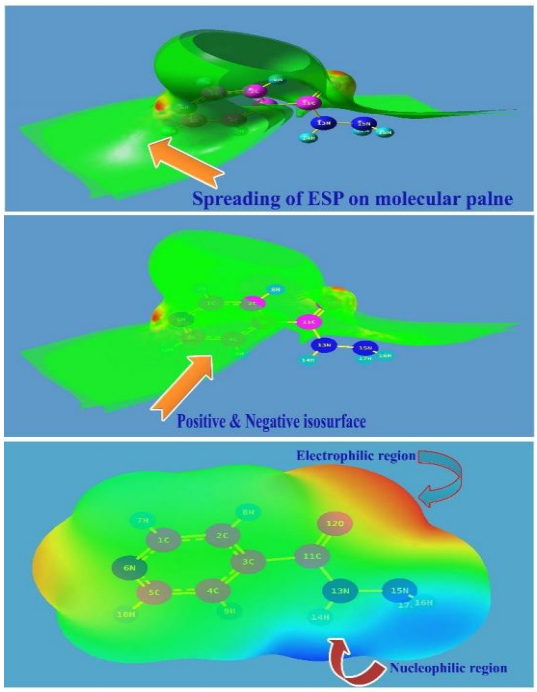

The two extreme ends of charge distribution was represented by the color code in the range between -7.66 a.u. (genuine red faded to yellow) to
7.66 a.u. (genuine blue faded to green). Generally, the negative region is mainly localized over the portion of highly electronegative atoms.

In this case, the electron bustle zone was captured over the O of carbonyl group, N of amino group and the N of pyridine ring. The moderate negative region was concealed over the pyridine ring and further decayed when moved towards H of ring. The protonic content was confined on the hydrogen zones over the amino group. It was abundant in around the edge of amino group and deficient in carbon bonded H. This well defined atmosphere was induced by hetero nuclear bond in ring and disorder on amino groups. Due to the electron pulling away from the ring, the electrostatic energy was found to be uniform at the centre part of the ring and acted as depletion energy grid. In each and every molecule, the number of homo and hetero nuclear bonds due to the strong ligand is root cause of the major property of the compound. In this case, the strong electrophilic- nucleophilic dipole was found between ring Carbonyl and amino groups. The out of plane ligand usually making strong receptor activity when docking is made. Here, carbonyl and amino group chain appeared as out of plane ligand which will be acting as good bridging action.

1.7. Chemical properties

The transition energy of Frontier molecular energy levels represented chemical properties and molecular reactivity descriptors of composite structure. The entire chemical parameters were presented in the Table 7. The asymmetric charge distribution was measured by the resultant dipole moment of the compound and it was found to be 4.70 and 3.97 dyne in IR and UV- Visible region respectively. The resultant dipole moment of the pyridine ring is found to be 2.64 dyne whereas the present compound was 2.06 and 1.33 dyne greater than pyridine ring which was due to the addition of functional group in the compound. This increment of dipole moment was ensured the charge depletion in the molecule where the pharmaceutical activity was induced much.

The energy gap of the frontier molecular orbitals measured usually, the chemical stability of the compound and was determined to be 2.71 and 2.31 eV in IR and UV-Visible region respectively. Both the values showed reasonable chemical stability and the compound would not be disintegrated by other toxic radiation. The electron affinity of the molecule is very important for the determination of the reaction ability of receptor protein and was found to be 7.283 which were elevated to the extreme and the reaction capability of the present compound is energetic.

The ionization potential of the compound is significant to evaluate consistency chemical-bond. The ionization potential was found to be 1.862 which was moderate and enough to maintain the chemical bond stability and molecular property. Generally, the chemical hardness is a scale of obstacle for transformation of charge whereas the electronegativity is measure of the tendency to attract electrons by inter-chemical bond. Here, both parameters were found to be 2.71 which was very low and able to have good reactive character and it was possible to add further add or alternate drug properties.

The exchange of energy between frontier molecular orbitals can be measured by electrophilicity index and is an indicator high degree of electron cloud. In this case, the electrophilicity index was recognized to be 3.857 eV, but the same was 3.05 eV for pyridine ring. The derived energy was high when compared with base ring which was due to the mono substitution of ligand groups. From this point of view, it was clear that, the maximum energy exchanged between ligand via ring for creating the antibiotic activity.

Here, the pyridine ring was the base compound and it was substituted by carbonyl and amino groups where the electrophilicity charge transfer of the compound was found to be + 1.687 which emphasized the maximum charge flow from ligand to ring. This also major cause of the present compound is an anti pyritic agent.

Parameter	Parameter	UV-Visible region	Electrophilicity charge transfer (ECT) (ΔNmax)A-(ΔNmax)B
Etotal (Hartree)	-472.435	-472.273	
EHOMO (eV)	7.283	7.019	
ELUMO (eV)	1.862	2.387	
ΔEHOMO–ΛYMO γαπ (ες)	5.42	4.632	
EHOMO-1 (eV)	7.572	7.373	-1.687
E_{LUMO+1} (eV)	1.035	1.274	
$\Delta E_{HOMO-1-\Lambda YMO+1\ \gamma\alpha\pi}$ (ες)	6.536	6.099	
Chemical hardness (η)	2.71	2.316	
Electronegativity (χ)	-4.572	-4.703	
Chemical potential (μ)	-4.572	-4.703	
Chemical softness(S)	0.184	0.215	
Electrophilicity index (ω)	3.857	4.775	
Dipole moment	4.706	3.978	

Table 7: Calculated energies, chemical hardness, electro negativity, Chemical potential, Electrophilicity index of Isonicotino hydrazide in UV-Visible region.

1.8. NBMO analysis

The electron cloud transition among non bonding molecular orbital abundantly involved in the inducement of the molecular property of composite molecule. The electron charge dislocation is purposively made by exchange of potential in terms of electronic energy among different entity of the composite for the development of particular drug activity. Such energy is laid down between lower energy of bonding orbital and higher energy of antibonding orbital [46]. The entire chemical property is depends upon the electronic potential is utilized for dislocating the electronic cloud for creating unique activity of the compound. Here, the non bonding molecular orbitals were urbanized by combining base and ligand groups. It was very important to identify the exchange of energy from which identity to which identity in the molecule.

Here, in ring system, the transition from NMBO of C1-C2 to C3- C11, C2-C3, C3-C4 and C5-N6 and they assigned to n-σ* in which 3.06, 2.82, 23.44 and 18.32 kcal/mol energy respectively were transferred from first ring to ring and chain in order to connect the major ligand groups. Among those transitions, within the ring, the maximum energy was transferred. Similarly, the n-π* transition was found from C1-N6 to C5 and C5-H10 within the ring system with 3.96 and 2.24 kcal/mol amount of energy. Here, such feeble amount of potential energy was utilized to stabilize charge level in ring system. The 4.43 and 2.29 kcal/mol amount of energy

used for n-σ* transitions from C3-C11 to N13-N15 and C1-C2. The reversible transition energy from ring was directed towards ligand for stabilizing the chemical property of the compound.

In same way, the transitions assigned to n-σ* from C3-C4 to C5-N6 and C1- C2 with utilization of 26.56 and 16.82 kcal/mol energy respectively. When compared with previous, it was very potential energy was consumed for retaining the charge levels within the ring system. The transition was assigned to n- π* from C11-O12 to C3-C11, C3-C4 and C11-O12 with the respected energy of 1.78, 3.49 and 0.82 kcal/mol within the ligand group. This energy was found to be very low which was utilized to stabilize the orbitals within the ligand system. From these transitions, it was cleared that, the considerable amount of energy was exchanged within the ring system, from ring to ligand and from ligand to ring system. When compared all the transitions, the maximum amount of energy utilized to transfer the electronic cloud within the ring system for inducing antibiotic property.

Transition	Donor (i)	Acceptor (j)	E2 kcal/mol	Ej – Ei au	F(i j) au
n – σ*	C1-C2	C3-C11	3.06	1.12	0.053
		C2-C3	2.82	1.28	0.054
		C3-C4	23.44	0.28	0.073
		C5-N6	18.32	0.26	0.062
n- π*	C1-N6	C5	3.96	1.87	0.077
		C5-H10	2.24	1.25	0.047
n – σ*	C1-H7	C2-C3	3.58	1.09	0.056
		C5-N6	4.72	1.06	0.063
n- π*	C2-C3	C3-C4	4	1.27	0.064
		C4-H9	2.91	1.14	0.051
n – σ*	C2-H8	C3-C4	4.32	1.08	0.061
		C1-N6	4.3	1.06	0.06
n – σ*	C3-C4	C2-C3	3.98	1.28	0.064
		C4-C5	2.58	1.28	0.051
		C5-N6	26.56	0.27	0.076
		C1-C2	16.82	0.29	0.064
n – σ*	C3-C11	N13-N15	4.43	0.97	0.059
		C1-C2	2.29	1.22	0.047
n- π*	C4-C5	C3-C4	3.05	1.28	0.056
		C3-C11	3.77	1.12	0.059
n – σ*	C4-H9	C2-C3	4.01	1.1	0.059
		C5-N6	4.22	1.08	0.06

Table 8: Non Bonding molecular orbital parameters of Isonicotino hydrazide

4.10 Polarizability and hyperpolarizability profile

The polarized and hyper polarized orbitals are reconstituted with respect to the existence of chemical force of attraction for the molecular stabilization make possible to induce the drug property and they can be measured by calculating the Polarizability and first order hyperpolarizability tensor as in the Table 9.

The calculated value of the dipole moment was found to be very high (4.76 Debye) since the number of hetero dipole pole moments were found to be higher order and it is enough to induce first and second order polarization. The major core of ligand groups were observed on the plane of molecule and results intensive polarization. The calculated showed that, the major entities were found to be on z coordinate of the compound which point out the arrangement of ligand chain. The calculated multi pole constants in different coordinates were tabulated among which the rich polarization constants were found (~55 a.u) in xx, yy and zz coordinates. This was the main cause of the obtaining the polarization constants with considerable amount. The calculated average Polarizability and anisotropy of the Polarizability was 126.48 x10^{-30}esu and 175.23 x10^{-30}esu, respectively. These values were so high and to be behind to set up strong bridge between ligand and ring group which stabilize the particular drug property.

Such high values also cause of the hyper polarization action and the hyperpolarizability β is one of the important key factors of strong molecular orbital interaction system which was the main source of the inducement of antibiotic activity. The B3LYP/6-311++G(d,p) calculated first hyperpolarizability value (β) is 790.26 x10^{-33}esu.

From this high value of result, it was clear that, the hyper asymmetrical polarization was empowered the stabilization of frontier molecular orbitals interaction for the stimulation of therapeutic activity.

Parameter	B3LYP6-31	B3LYP 6-311	Parameter	B3LYP 6-31	B3LYP 6-311
α_{xx}	-62.2366	-62.2202	β_{xxx}	83.0242	82.2134
α_{xy}	-13.2356	-13.0668	β_{xxy}	-23.1768	-22.6226
α_{yy}	-54.5181	-54.4756	β_{xyy}	-6.5732	-6.5914
α_{xz}	5.8565	5.6956	β_{yyy}	-11.8097	-11.7657
α_{yz}	2.7749	2.8541	β_{xxz}	16.0431	15.5269

α_{zz}	-58.7065	-58.6774	β_{xyz}	-0.2716	-0.2670
α_{tot}	126.489	126.343	β_{yyz}	3.5057	3.4570
$\Delta\alpha$	175.234	175.180	β_{xzz}	13.7065	13.6889
μ_x	1.7538	1.7653	β_{yzz}	-1.3945	-1.4333
μ_y	-3.9371	-3.8851	β_{zzz}	2.1363	2.0861
μ_z	2.0368	1.9839	β	790.260	790.903
μ	4.7671	4.7060			

Table 9: The dipole moments μ (D), the polarizability α(a.u.), the average polarizability α_o (esu), the anisotropy of the polarizability Δα (esu), and the first hyperpolarizability β(esu) of the compound; Isonicotino hydrazide.

1.9. Thermodynamic function analysis

Normally, the thermo dynamical analysis on aromatic compound is very important since they offer the important information regarding the thermodynamic character of chemical reactivity. [45]. Thermodynamic functional parameters were depicted in the Table 10. The calculated entropy, specific heat capacity and enthalpy were found to be varied positively with temperature. When the temperature increased from 100K to absolute temperature 298.15, the functional parameters were varied unhurriedly whereas from 350 to 1000K, the thermodynamical functions recognized to be linear pattern and rather constant at maximum temperature. This view of variation showed the consistent chemical reactivity and considerable chemical hardness of the present compound. The Gibbs free energy has negative temperature coefficient constantly and it was found to be consistently increased with respect to temperature. This elevated view of the Gibbs free energy showed the flat character of the continual chemical reaction of compound.

T(K)	C^0_{pm}(calmol^{-1} k-1)	S^0m(cal mol^{-1} K^{-1}	ΔH^0_m (kcal mol^{-1})	Gibbsfreeenergy $\Delta G = \Delta H - T\Delta S$ KJmol^{-1}
100	282.07	68.38	4.87	-6833.13
200	340.96	106.12	13.58	-21210.4
298.15	390.68	145.8	25.93	-43444.3
300	391.58	146.56	26.2	-43941.8
400	439.16	185.35	42.83	-74097.2
500	484.19	218.4	63.07	-109137
600	526.47	245.23	86.3	-147052
700	565.96	266.89	111.95	-186711
800	602.79	284.61	139.55	-227548
900	637.19	299.33	168.77	-269228
1000	669.38	311.74	199.34	-311541

Table 10: Specific heat capacity, entropy and enthalpy at different temperatures for Isonicotinohydrazide.

1.10. Molecular Docking Study

Anthranilate phosphoribosyltransferase (AnPRT) belongs to phosphoribosyltransferase (PRT) enzyme family and is an attractive enzyme in the field of drug discovery and tuberculosis therapy, since it is essential for the biosynthesis of tryptophan in Mycobacterium tuberculosis (Mtb) [48]. Each chains of AnPRT consist of a smaller N-terminal domain and a larger C-terminal domain. C-terminal domain contains a central seven-stranded β- sheet surrounded by eight α-helices [49] and N-terminal domain consists of six α-helices. In each chain, two anthranilate binding sites were present, one of which is located in the hinge region between the N-binding site and an another site situated farther to the phosphoribosyl group of 5′-phosphoribosyl-1′-pyrophosphate (PRPP). Inhibitors like anthranilate and flouroanthranilate have been observed to bind to Mtb-AnPRT in the abovementioned active sites, located at the entrance to the anthranilate tunnel [50]. In order to understand how the title molecule inhibits and hence increases the catalytic efficiency of Mtb-AnPRT enzyme, a docking study was performed to fit the title compound into the active centre of the Mtb- AnPRT enzyme. High resolution crystal structure of Mtb-AnPRT (PDB ID: 1ZVW) [51] was used as the receptor enzyme and AutoDock4 software was used to perform all molecular docking simulations. For the calculations, water molecules were removed and polar hydrogen atoms were added to the receptor molecule. The active centre around the N-binding site of the receptor was defined by incorporating all amino acid residues within a radius of sphere 7 Å centered on the co-crystallized inhibitor (PRPP).

In order to model the interaction pattern between receptor and the ligand, Lamarckian Genetic Algorithm (LGA) available in AutoDock was employed. Out of ten docked confirmations obtained, one which has lowest binding energy (-7.26 kcal/mol) was selected and analyzed for detailed interactions using Discover Studio Visualizer4.0 software and Pymol. The predicted binding mode for the title molecule showing significant inhibition and the amino acid residues which form hydrogen bonds with the ligand were labeled in Figure 11. The title compound shows hydrogen bond formation with residues Asp111, Thr115 and Ser143. The electrostatic contacts are driven by Mg2+ ions present in the active site. The amino group in the title molecule acts as hydrogen donor and forms hydrogen bond with Asp111, while it acts as hydrogen acceptor in making hydrogen bond with Thr115. The docked binding pose of the title molecule also speculates the formation of another strong hydrogen bond with residue Ser143 where carbonyl oxygen is acting as hydrogen acceptor. Surface representation of the receptor with the ligand bound is shown in Figure12 from which it can be seen that, the ligand is bound well inside the active pocket of the enzyme. Estimated free energy of binding shows that the title compound has good affinity towards the Mtb-AnPRT enzyme. The results from the molecular docking study revealed that the title molecule may inhibit catalytic efficiency of Mtb-AnPRT enzyme.

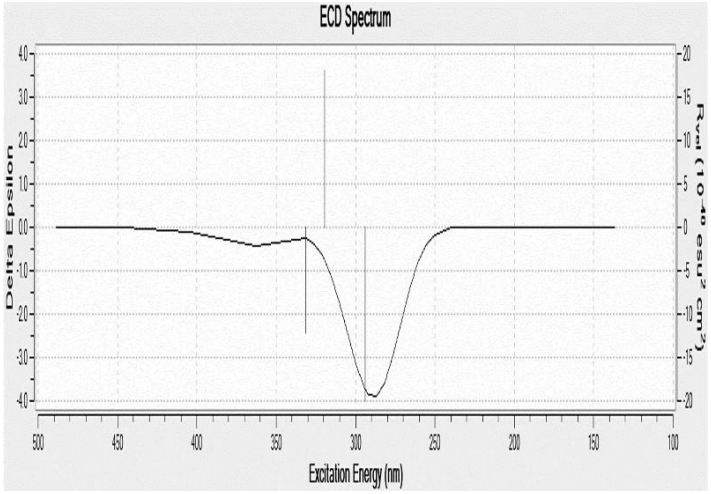

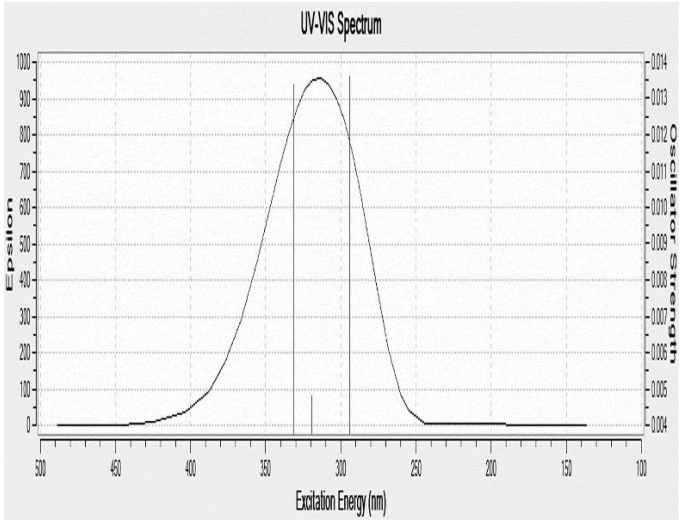

2. Conclusion

Molecular spectroscopy investigation has been performed to investigate the compound's chemical and pharmacological properties. In this case, every study conducted on the molecule demonstrated the underlying source of the antibacterial property. The active nature of the molecule's constituent parts was highlighted by the vibrational analysis, which also verified the location and existence of every bond in the compound. It was discovered that the energy distribution over various chemical entities preferred the frontier molecular orbital interaction profile. The chromophores' activity from electronic excitation absorption for the functional groups was emphasized by the UV-visible analysis. The background factors that led to the induction of antibiotic properties were identified, and the current molecule was found to be pharmaceutically active. Molecular docking studies were used to test the title molecule's inhibitory catalytic effectiveness.

Citations :

[1] Centers for Disease Control, "TB Guidelines: Treatment." cdc.gov, 2016.
[2] Berning, S.E., Peloquin, C.A., Vaccines and Antimicrobial Therapy, Williams and Wilkins, Baltimore, 1998; Yu V., Merigan T., and Barriere S. (eds.).
[3] West-Ward Pharmaceutical Corp., Eatontown, N.J., 2014.
[4] Mikart G.A., Inc., Atlanta, 2015.
[5] Young DB, Brennan P.J. Anti-tuberculosis Agent Handbook, Tuberculosis 88, 85–170 (2008). Y.L. Janin, Review of Anti-TB Drugs, Bioorganic Medical Chemistry, 15:2479–2513 (2007).
[7] G. L. Middlebrook (1953) Cohn, Science, 118, 297–299.
[8] Fourth-generation fluoroquinolones in tuberculosis, Rieder H.L. (2009), Lancet (373)1148–1149.
[9] http://www.rxlist.com/clinicalpharmacology//html/isoniazid-drug.
[10] Pandian, G.V., Ramalingam, S., Jobe Prabakar, P.C., and P. Anbusrinivasan (2016), Journal of Physics and Chemistry of Solids 91:55–68.
[11] Spectrochimica Acta Part A: Molecular and Biomolecular Spectroscopy 149; 216-230 (Xavier, S., Periandy, S., 2015).
[12] Moorthy, N., Govindarajan, M., Ramalingam, S., Jobe Prabakar, P.C., et al. Journal of Physics and Chemistry of Solids 95(2016)74–88.
[13] Hiremath.C.S, Tonannavar.J, Jayashree Yenagi, Spectrochimica Acta Part A 68, (2007) 710–717.
[14] Journal of Molecular Structure (1099) 463-481 Manzoor Ali, Gene George, Ramalingam, S., Periandy, P., and Gokulakrishnan, V. (2015).
[15] Phys. Rev. (56) 340 Hellmann, H. and Feynman, R.P. (1939).
[16] In 1966, Das, G. and Wahl, A.C., J.Chem. Phys. (44) 87
[17] Chem. Phys. J. (48) 252, Kestner, N.R. (1968).
[18] Spectrometric Identification of Organic Compounds, Silverstein, M., Clayton, Basseler, G., and Morill, C., Wiley, New York, 2001.
[19] Spectrochimica Acta Part A 85 (2012) 145-154; Ahmet Ataca, Mehmet Karabacak, Caglar Karaca, and Etem Kose. Acta A 74 (2009) 375–384; Arjunan.V, Aravanan.S, Ravindran.P, Mohan.S. Spectrochim.
[21] George Socrates, Raman and Infrared Characteristic Group Frequencies (Tables and Charts), John Wiley & Sons, Ltd. (2001).
[22] Atlas of Spectra of Aromatic and Heterocyclic Compounds, A. F. Ardyukova et al., Nauka Sib. Otd., Novosibirsk,
[23] Church F. M. and Cook G. L. (1957) l. Phys. Chem, (61) 458.

[24] Quart. Rev. (1959) 13; 353, Katritzky A. R.
[25] Spectrochim. Acta, 1973, 29A, 293, J. H. S. Green and D. J. Harrison.
Mol. Struct. (655) 89–95; P. Koczon, J.Cz. Dobrowolski, W. Lewandowski, and A.P. Mazurek, J. (2003).
[27] Spectrochimica Acta Part A (77) 73–81 (1910) Ramalingam, S., Periandy, S., and Mohan, S.
In 1993, Wang, Saebo, and Pittman published a study in the Journal of Molecular Structure (Theochem.) (281) 91–96.
[29] Arjunan, V., Mohan, S., and Puviarasan, N., Turkey Journal of Chemistry 26 (2002) 323.
[30] Interpretation of Infrared Spectra: A Practical Approach, Coates, J., and Meyers, R.A., John Wiley and Sons Ltd., Chichester, 2000.
[31] Journal of Molecular Structure (Theochem.) (362) 325; Jensen, J.O., and Hameka, H.F. (1996).
[32] In 1991, the Journal of Raman Spectroscopy (22) 141, J.R., Bergana, M.M., Phan, H.V.
[33] Introduction to Infrared and Raman Spectroscopy, Colthup, N.B., Daly, L.H., & Wiberley, S.E. (1964), Academic Press, Inc., London
[34] A Systematic Approach to Infrared Spectral Interpretation, Smith, B. (1999), CRC Press, Washington, DC
[35] Spectrochimica Acta A (56) 119–126; Ts.M. Kolev, B.A. Stamboliyska (1999).
[36] Spectrosc. (44) 331–342; Sett.P, Misra.T, Chattopadhyay.S, A.K. De, Mallick.PK, Vib (2007).
[37] Jag Mohan (2010) Organic Spectroscopy: Principles and Applications, Narosa Publications, New Delhi, Second Edition
[38] The Indian Journal of Pure and Applied Physics, 30 (764-770), Ahmad, Mathew, and Verma, P.K. (1992).
[39] Karthikeyan, N., Joseph Prince, J., Ramalingam, S., and Periandy, S. (2014), Spectrochimica Acta Part A: Molecular and Biomolecular Spectroscopy (124) 165–177.
[40] Balc. M. (2005) Basic p1 sH and p13 s CNMR spectroscopy. Stockholm: Elsevier, 1st ed. (12)427.
[41] Breitmaier, E. (2002), NMR structure elucidation in organic chemistry: a useful manual. Wiley, Chichester, West Sussex, England, 3rd rev. ed., (xii), 258.
[42] Yvesand Jean and Francois Volatron. A Brief Overview of Molecular Orbitals. Oxford University Press, 2005
[43] In the Journal of Molecular Structure (1106) 37–52, Manzoor Ali.M, Gene George, Ramalingam.S, Periandy.S, and Gokulakrishnan.V (2016).
[44] Karr, G. (2005), Molecular spectroscopy: Fundamentals and Uses, Narosa Books
[45] Spectrochimica Acta Part A: Molecular and Biomolecular Spectroscopy (140) 85-95; Caglar Karaca, Ahmet Atac, and Mehmet Karabacak (2015).
[46] Anslyn, V., Eric, Dougherty, A. Dennis (2006), University Science Books 841–842, Modern Physical Organic Chemistry.
[47] In the Journal of Molecular Structure (1099) 463–481, Manzoor Ali.M, Gene George, S. Ramalingam, Periandy.P, and Gokulakrishnan.V (2015).
Baker, E.N., Lott, J.S., Parker, E.J., Evans, G.L., Cookson, T.V.M. (2015), Biochemistry (54) 6082-6092.
[49] Lee, C.E., Javid-Majid, F., Goodfellow, C., et al. (2006) J. Mol. Biol. (355) 784-797.
[50] Bulloch, E.M.M., Evans, G.L., and Gamage, S.A. (2014), J.S. Lott, Chem. Bio. Chem. 15 852-864.
[51] Marino.M, Deuss.M, Svergun D.I. (2006), J. Biol. Chem. (281) 21410-21421.